Finite Element Analysis of a Transcranial Electromagnetic Stimulation Case Study

A Major Qualifying Project Report

Submitted to the Faculty

Of the

WORCESTER POLYTECHNIC INSTITUTE

In partial fulfillment of the requirements for the

Degree of Bachelor of Science

By

Edward Burnham

Submitted to

Professor Sergey Makarov

April 20, 2017

Abstract

Transcranial magnetic stimulation (TMS) is a burgeoning field of medicine currently under intense study exploring its therapeutic and diagnostic applications. One such study at the Massachusetts General Hospital (MGH) concerns a patient who had a seizure while undergoing TMS treatment for medication-resistant depression. The purpose of this Major Qualifying Project was to create an accurate model of the patient from T1 and T2 magnetic resonance imaging (MRI) data using a complex toolchain of medical imaging and mesh processing software. ANSYS Maxwell was used to conduct a finite element analysis (FEA) of the patient's unique cranial geometry to calculate the electric field inside the cortex during a simulated TMS procedure. This analysis was done to gain insight into the cause of the patient's seizure. Additionally, this project aimed to make recommendations for the process of rapid 3D surface mesh generation from T1 and T2 MRI data. This recommendation is significant in the safety and individualized setup of TMS procedures.

Acknowledgments

I would like to express my deepest gratitude to the following people for their support on this project:

- Professor Sergey Makarov for your knowledge, trust, and mentorship.
- Dr. Aapo Nummenmaa for the opportunity and guidance you gave.
- Dr. Greg Noetscher for your support and advice throughout the project.
- Jerry Li, Harshal Tankaria, Janakinadh Yanamadala, Mariya Zagalskaya, and David Kelly for your valued contributions and comradery.
- The WPI Electrical and Computer Engineering department for enriching all aspects of my life.

Table of Contents

Table of Figures

Table of Tables

Background

Transcranial Magnetic Stimulation

Transcranial magnetic stimulation (TMS) is the induction of an electric field in the brain by a pulsed magnetic field generated using an excited coil placed close to the skull [1]. This electric field can depolarize neurons and thereby modulate cortical function [2]. Several TMS devices have been approved by the FDA as a noninvasive treatment for medication-resistant depression [3]. Stimulation devices typically consist of a transducing coil attached to a discharge system capable of delivering 400 V-3 kV and 4 kA-20 kA [4]. This results in 1.5-2.0 Tesla (T) at the face of the coil and can induce electric fields in the brain up to approximately 150 V/m. It is assumed that the field can activate neurons at a depth of 1.5-3.0 cm [5]. TMS treatments are typically delivered in trains of pulses. There are 4 key parameters which define TMS dosing: train duration, inter-train interval, intensity, and frequency. A course of treatment may consist of many 30-minute TMS sessions and may include maintenance sessions [6].

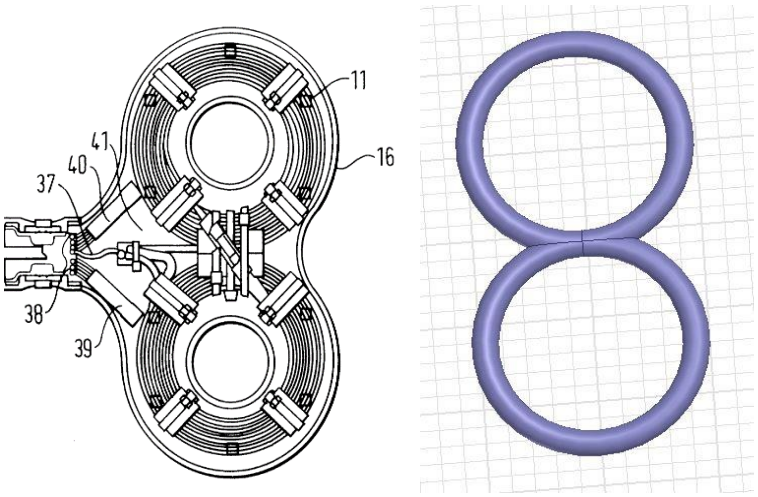

Figure 1. On left is an example of a TMS coil from US Patent 6179770 [7] and on right is the coil geometry used in this project's simulations.

Applications of TMS

In addition to its use in treating depression, TMS has applications in research, discovering associations between stimulated brain regions and their resulting behaviors. These links could then be used diagnostically to evaluate damage from stroke, and other injuries or disorders affecting neurons [8]. Additionally, there is evidence that it may be useful in treating neuropathic pain [9]. TMS has been suggested for use in the treatment of maternal depression thereby bypassing fetal exposure to drugs, but further study is required [10]. To this end, there are many clinical trials investigating TMS treatment for a variety of neuropsychiatric disorders [11].

Safety of TMS

A single pulse of TMS has been said to raise temperatures in the brain under 0.1 C [12]. High rates of blood flow in the brain provide a safety margin for brain-temperature increase [13]. TMS coils heat up significantly, however, and have the potential to induce currents in any implants or conductive materials present in the subject, causing additional heating and unintended cortical stimulation. Especially concerning is conductive surface electrodes made of silver or gold which can reach temperatures of 50-55 C, causing skin burns [14]. TMS may also damage the internal circuitry of implanted devices such as cochlear implants, deep brain stimulation systems, and cortical stimulation electrode arrays, causing them to malfunction. A meta-analysis concludes that TMS can be applied safely to patients with implanted stimulators of the nervous system if the TMS coil is not near the internal pulse generator [6]. Chronic electromagnetic field exposure possible during TMS treatment is well under accepted levels [15].

The most severe acute adverse effect of TMS treatment is induced seizures. Our case of accidental seizure occurred even after the definition of safety limits and the establishment, through several reported cases, that TMS can cause seizures [6]. A review of safety in TMS treatment for epilepsy recorded a 1.4% crude per-subject risk to develop a seizure, though this statistic is likely skewed *low* due to the presence of antiepileptic drugs in the subjects [16]. The risk of seizure during TMS treatment has been shown to be less than 1% in non-epileptic subjects. Other circumstances may increase the probability of seizure such as medications, diseases such as autism or stroke, and a history of seizures [6].

An effective way to understand the risks associated with TMS is to examine the questionnaire asked of patients prior to treatment. From *Clinical Neurophysiology*, the following is an updated screening questionnaire before TMS:

1. Do you have epilepsy or have you ever had a convulsion or a seizure?

2. Have you ever had a fainting spell or syncope? If yes, please describe in which occasion(s)?

3. Have you ever had head trauma that was diagnosed as a concussion or was associated with loss of consciousness?

4. Do you have any hearing problems or ringing in your ears?

5. Do you have cochlear implants?

6 . Are you pregnant or is there any chance that you might be?

7. Do you have metal in the brain/skull or elsewhere in your body (e.g., splinters, fragments, clips, etc.)? If so, specify the type of metal.

8. Do you have an implanted neurostimulator (e.g., DBS, epidural/subdural, VNS)?

9. Do you have a cardiac pacemaker or intracardiac lines?

10. Do you have a medication infusion device?

11. Are you taking any medications? (Please list)

12. Did you ever undergo TMS in the past? If so, were there any problems?

13. Did you ever undergo MRI in the past? If so, were there any problems?

A patient saying “yes” to any one of these does not preclude them from TMS treatment, however the risk/benefit ratio of a “yes” answer should be examined by the researcher or physician conducting the TMS procedure [17].

Uncertainty in TMS Setup

Currently, there is a great deal of uncertainty in the setup of the TMS procedure. Parameters which vary are location of the coil, size of the patient’s head, and conductivities of the tissue layers of the head, which all contribute to determining the patient’s threshold of stimulation [43]. The electric field distribution is susceptible to changes in these parameters and it is important to accurately target the cortical region of interest [6]. Therefore, it is important to quantify these parameters and minimize the uncertainty of the TMS procedure for each session.

Coil targeting of the dorsolateral prefrontal cortex in depression clinical trials have used scalp landmark methods, which is a combination of visual targeting and elicitation of a motor twitch in the subject’s hand [44]. Frameless stereotaxy is also used to position the coil to anatomically defined targets [6]. It has been demonstrated that improved targeting using MRI in TMS for depression yielded better treatment outcomes [18]. However, MRI targeting is impractical for most TMS users.

Guidelines for Induced Currents

The International Commission on Non-Ionizing Radiation Protection (ICNIRP) provides guidelines for exposure levels to time-varying electric, magnetic, and electromagnetic fields [19, 20]. These guidelines serve to protect people from the adverse health effects of nonionizing

radiation (NIR) up to 300 GHz. Currents exceeding those of human-originating bioelectric signals in tissues cause many adverse physiological effects which increase as induced current density increases [4]. At current densities of 10-100 mA/m^2 modulation of brain cognitive function occurs. For frequencies of 10 Hz to 1 kHz, when current density exceeds 100 mA/m^2, thresholds for neuronal stimulation are exceeded and potentially life-threatening effects such as respiratory failure may occur [19]. The possibility of permanent tissue damage becomes greater with prolonged exposure to strong induced current densities [4]. The ICNIRP guidelines for exposure to NIR in the band of 1-110 kHz for the human head and trunk are current densities below f/500 mA/m^2, where f is the signal frequency in hertz. At 5 kHz, the maximum exposure recommended is 10 mA/m^2 [20]. This estimate can also be stated in terms of the induced electric field by dividing current density by conductivity [4].

Computational Electromagnetics

Overview

Computational electromagnetics (CEM) is a broad category of processes that attempt to link electromagnetic theory and novel experimentation to accurately predict the behavior of electromagnetic systems through simulation. Researchers use this tool to simulate electromagnetic effects on discretized physical geometry in a parameterized environment. An example of discretized geometry as it pertains to this project is shown in Fig. 2. Maxwell's equations are simplified (i.e. using boundary conditions) and solved numerically to find the electromagnetic wave propagation through a geometry in a reasonable time frame with available computing power.

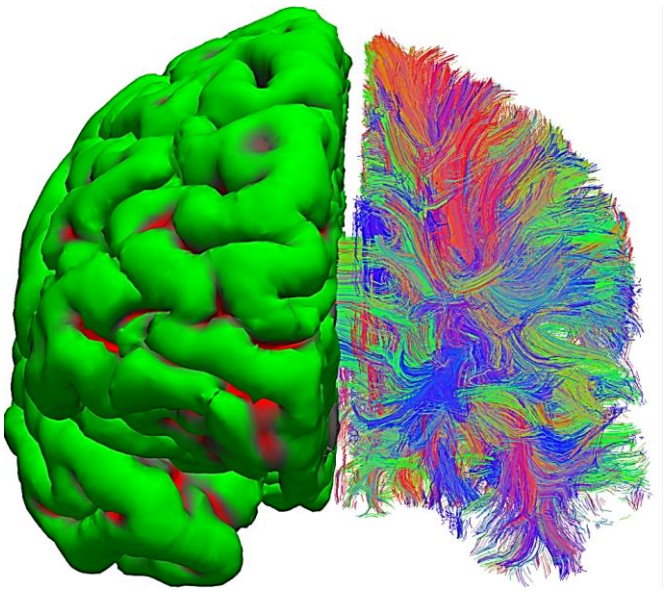

Figure 2. An example of discretized geometry in two forms. The left hemisphere is represented by a surface CAD model. The right hemisphere uses a neural-fiber model.

Computational electromagnetic procedures have gained traction within several fields such as antenna design, and other communication systems, but most notably within the medical community and medical device design [21]. Cellular phone manufacturers, automotive manufacturers, magnetic resonance imaging, functional brain imaging, and transcranial magnetic stimulation are a few examples of the myriad applications of electromagnetics within the scope of medicine. Computational electromagnetics has been identified as an influential tool during the development of medical devices and medical device applications by the Food and Drug Administration (FDA) [22].

There are several solution methods for CEM and it is important to choose a technique appropriate for the problem. A poor choice of CEM method would mean inaccurate results or impractically long computation times. Furthermore, each method also has specific discretization strategies, involving geometries and basis functions, which have implications in development and computation time [42]. For this project, we used the finite element method (FEM) with

discretized geometry represented by a 3D CAD surface mesh model and vector basis functions [23].

Finite Element Method

The FEM is a process that uses numerical methods to approximate solutions to differential equations. It is important to note that FEM is not limited to applications in computational electromagnetics and can be applied to study other physical phenomena such as mechanical stress and fluid flow. One of the advantages of the FEM is that the technique allows various governing equations to be adapted to it and regardless of this, the steps to the solution remain the same. However, a disadvantage to FEM compared to other CEM methods is the lack of an explicit solution [24]. Rather, the problem is realized with a system of linear equations and solved iteratively until convergence takes place [42]. This iterative numerical method can increase the need for computational resources significantly and solution time can be lengthy.

One additional advantage to FEM is an adaptive mesh refinement procedure. When employed in conjunction with unstructured meshes like a 3D CAD surface mesh, the accuracy of the geometry can be adaptively increased until convergence is reached [42]. This results in a significant reduction in computation time without sacrificing the accuracy of the simulation. Materials of various properties are modeled in the method as well, with alterations of the equations relating to the behavior of certain terms [25].

From [24, 25], the steps for the Finite Element Method include the following:

1. Separate the domain of the solution into non-overlapping, adjacent subdomains

2. Choose the applicable basis function to interpolate the solution variable over the subdomains
3. Estimate the solution variable so that the sum of each element's influence on that variable results in the overall solution
4. Develop the solution using common methods such as the discontinuous Galerkin family of numerical methods [26]
5. Solve the resulting system of equations after application of the boundary condition
6. Post-process the results and check for validity

Furthermore, one possible example for the governing equation for a one-dimensional boundary value problem (where Ψ is the solution variable, with material characteristics α and β, and if applicable, forcing function, f) is:

$$-\frac{d}{dx}\left(\alpha\frac{d\psi}{dx}\right)+\beta\psi = f \quad \text{(a)}$$

With the governing equation and the discretized solution domain defined, a basis function (otherwise known as an interpolating function or shape function) must be chosen. The Lagrange basis equation, or the basis for quadratic polynomials, for example, is shown in Eq. (b):

$$\ell_j = \prod_{i=1}^{n} \frac{x - x_i}{x_j - x_i} \quad \text{(b)}$$

In Eq. (b), note that *n* is the number of nodes and when *i* = *j*, the result is disregarded. Next, we generate an estimate of the solution variable so that the sum of each element's discrete solution is equal to the solution variable over the entire domain; following the example, this can be formulated in basis function form as:

$$\tilde{\psi} \cong \tilde{\psi} = \sum_{j=1}^{n} \tilde{\psi}_j N_j \quad \text{(c)}$$

When Eq. (c) is replaced into Eq. (a), we obtain an estimate of the solution in Eq. (d).

$$-\frac{d}{dx}\left(\alpha \frac{d\tilde{\psi}}{dx}\right) + \beta\tilde{\psi} = f \quad \text{(d)}$$

A minor variance between the numerical and analytical solution is found when Eq. (d) is set to zero. This variance is referred to as the residual, which is used when formulating the solution, and is shown in Eq. (e).

$$r = -\frac{d}{dx}\left(\alpha \frac{d\tilde{\psi}}{dx}\right) + \beta\tilde{\psi} - f \quad \text{(e)}$$

When formulating the solution using methods like the Galerkin Method of Weighted Residuals, the goal is to force the residual to zero over the solution domain. This is achieved by choosing coefficients or weighting functions and then integrating the weighted residual.

Once every element in the system is characterized by the Galerkin Method of Weighted Residuals, they are collected together into a system of linear equations representing the entire solution domain [24]. The final calculation step is performed by imposing the boundary conditions, like Dirichlet or Neumann types, which are used to simplify and produce a well-conditioned system of linear equations [24]. Post-processing is done to validate results and associate derived quantities to the discretized geometry. And, if the error value is too great than more adaptive passes may be performed, resulting in a finer mesh with more tetrahedra, and therefore greater accuracy [42].

Computational Modeling of Humans

Overview

Computational modeling of humans concerns the creation of discretized geometry of the human body for use in finite element analysis (FEA). The goal is to create models for use simulation to better understand the interaction of physical fields and forces on the human body. This has a particularly interesting application in the design and validation of medical devices and in better understanding multifaceted biomedical problems [27]. It is well understood that computational modeling of humans can accelerate research by assisting scientists in conducting many simulated experiments to determine which potentially costly physical experiment will best illustrate the problem being researched [21]. Because of this, computational human models have

become a significant part of biomedical research and many full-body models have been completed to date [29].

Human Model Construction

In general, human models are created in one of two discretization schemes which have implications for the types of CEM problems to be solved, model development in terms of process and time, and it determines compatibility with commercial FEA solver packages [42]. One type is voxel models, which is the most commonly used scheme for commercial human CEM models [28]. The other type is a CAD model, which we use in this project. Voxel models are preferred as human CEM models because they easily represent non-homogeneous tissue regions, creating them from source images without the immense amount of processing required by a CAD model. Moreover, CAD models, despite their drawbacks in terms of creation and processing time, have a mathematical advantage: they can give a linear or polynomic approximation, as opposed to a staircase approximation for the voxel model [29]. Additionally, CAD models can be deformed and are able have their resolution be adaptively refined [30].

Segmentation is a process of creating voxel or CAD CEM models from a set of images. Fig. 3 illustrates the process of manual segmentation, which is recognized as the industry standard [29]. In Fig 3a, an image of a patella is outlined to capture its geometry. Repeating this process on each image while moving upward in the z-direction, a point cloud like the one seen in Fig. 3b is generated. From the point cloud, either a voxel model (Fig. 3d) or a CAD model (Fig. 3c) may be created by connecting the points, in the case of a CAD model, or by creating voxels based on point location in the voxel model. A manual segmentation effort for a single model can

be measured in man-months or years [31]. As a result, there are also semi-automatic and automatic segmentation algorithms which use pixel contrast and probabilities to trace the boundaries of tissue geometry [32].

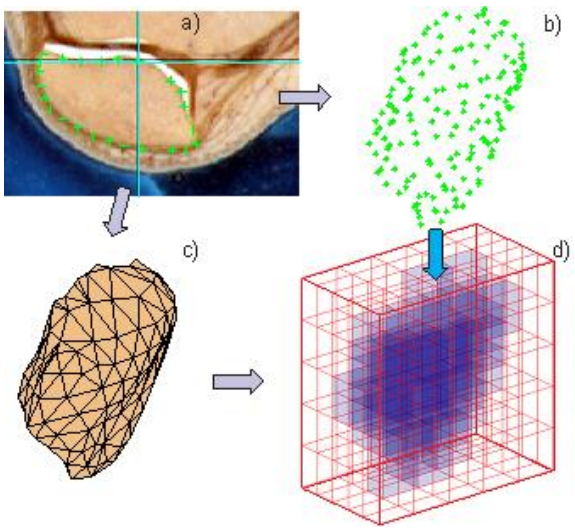

Figure 3. Illustration of segmentation procedure with CAD and voxel comparison.

Specific Parameters for CAD Models

Because we will use a CAD model in this project, we will discuss some of the parameters necessary for a functional CAD model for CEM use. First, a 3D triangular mesh representing a solid object must have no holes. Secondly, the mesh must be strictly 2-manifold [29]. A mesh is considered 2-manifold if every edge is manifold with only two triangles attached. Any deviation from this parameter results in an invalid mesh. Three examples of manifoldness are illustrated in Fig. 4.

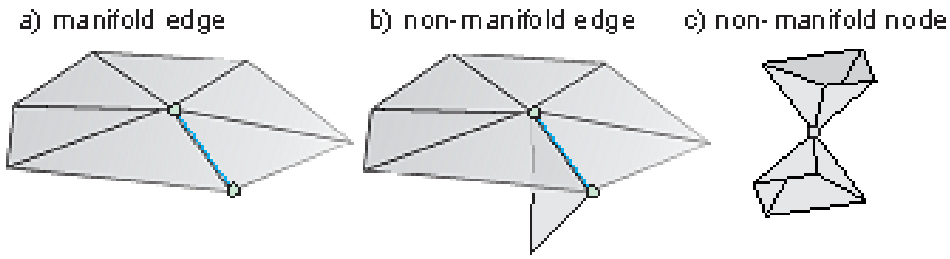

Figure 4. Illustrations of a) manifold edge, b) non-manifold edge, c) non-manifold node.

In addition to conditions related to the mesh itself, when multiple meshes representing different tissues are compiled into a larger model, the meshes must not intersect with each other [42]. Meshes fully enclosed within another mesh are fine. Usually the contact regions, where meshes must be extremely close without intersecting, are discovered through validation and corrected manually by slightly moving nodes in the direction opposite the contact region [42]. An example image of an intersected triangle as it would appear in ANSYS Maxwell's mesh validation tool is shown in Fig. 5.

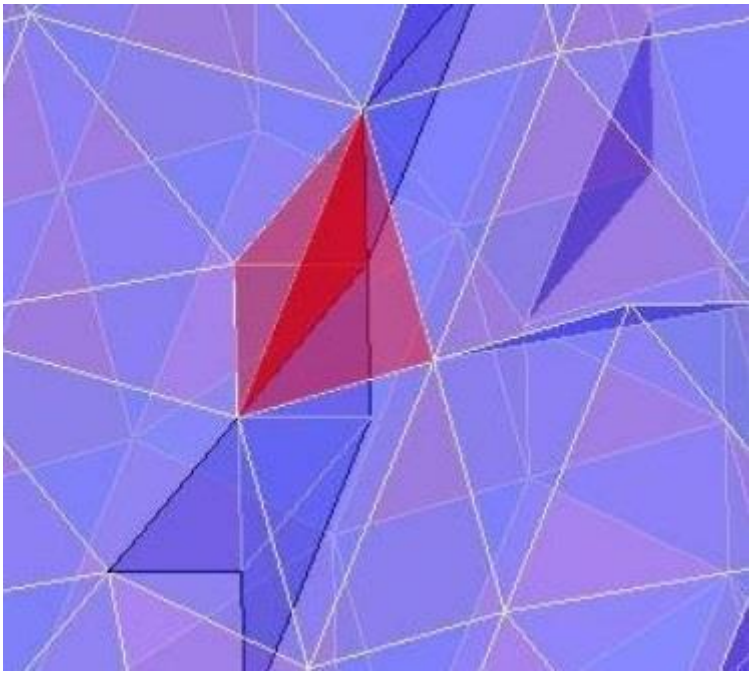

Figure 5. Intersected triangle in ANSYS Maxwell's mesh validation tool.

Mesh Refinement and Validation

After segmentation occurs, the mesh will go through a process of refinement to gain certain desirable characteristics. Decimation is performed to reduce the number of triangles in the model [33]. When a model is generated through segmentation, it may have up to hundreds of times the number of triangles desired. It may be infeasible to run a simulation on a mesh of that resolution using the computational resources available, therefore decimation is necessary. Smoothing is then performed to remove the sharp edges and improve triangle quality. Triangle quality is a measure of the acceptability of a triangular mesh for FEA simulations based on ratios of the geometric properties of the triangles [35]. We will use this ratio to measure the metric of minimum triangle quality, which is the value of the lowest quality triangle in the mesh. Minimum edge length of a triangle is another metric which is tracked to determine worst-case triangle properties which may affect simulation accuracy [42].

An algorithm such as Laplacian smoothing may be used in which a new vertex location is defined based on regional information for each vertex in a neighboring mesh [36]. Intersection and triangle quality issues are resolved using mesh processing tools such as MeshLab and ANSYS Space Claim. An example of one triangle quality issue, overconnected edges, which can be resolved in SpaceClaim is shown in Fig. 6. Other types of intersection and quality issues which are resolved in the refinement and validation process are self-intersections, holes, non-manifold nodes and vertices, spikes, fold overs, micro tunnels, and near-degenerate triangles [37].

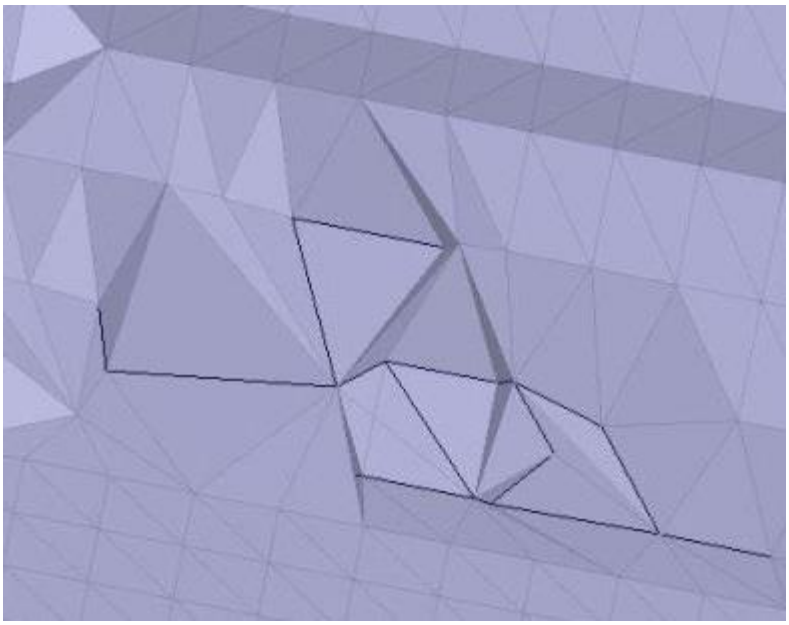

Figure 6. Overconnected edges as they appear in ANSYS SpaceClaim.

Dielectric Properties

In computational electromagnetics, models are described with their relative conductivity and permittivity of their tissues as functions of frequency. The standard data set from 10 Hz to 100 GHz for most human tissues was the work of C. Gabriel supported by the US Air Force Research Laboratory [29]. Samples for dielectric properties are taken both in-vitro and in-vivo; the only dielectric properties taken in-vivo are surface level samples, whereas after death, in-vitro, researchers able to gather samples of subsurface tissue such as white matter. Whether the in-vitro or in-vivo mechanism yields a significant difference, a difference that could potentially invalidate the results of a simulation, is still up for debate.

For the purposes of this project, the following tissues were used with their respective dielectric properties at a specific frequency of 5 kHz. The dielectric parameters are based on the Gabriel dispersion relationships [34].

Tissue	Source	Permittivity (F/m)	Elec. Cond. (S/m)
Skin	Skin (Dry)	1.13E+3	2.01E-4
Skull (Cortical Bone)	Skull (Cortical Bone)	8.40E+2	2.03E-2
Cerebrospinal Fluid	Cerebrospinal Fluid	1.09E+2	2.00E+0
Brain (Grey Matter)	Brain (Grey Matter)	4.23E+4	1.10E-1
Brain (White Matter)	Brain (White Matter)	2.09E+4	1.10E-1
Blood	Blood	5.23E+3	7.00E-1

Table 1. Table of Material Properties used in this Project - Permittivity and Electrical Conductivity at a frequency of 5kHz.

Methodology and Results

Case Study & Problem Statement

A Massachusetts General Hospital (MGH) case study concerning a patient who had a seizure while undergoing treatment for medication-resistant depression is the motivation for this project. The patient had an abnormality in his cerebral cortex, specifically in the region targeted by the TMS procedure. We received T1 and T2 (contrasted) magnetic resonance imaging (MRI) images from MGH and were tasked with creating a model of the human head and performing

FEM simulation to approximate the **E** field produced by the procedure. In addition to creating the model and performing simulations, we made recommendations for a process of rapid 3D surface mesh model generation, which would be of great benefit to the safety and individualized setup of a TMS procedure.

Model Development

Model development is the product of a large toolchain that includes SpaceClaim, MATLAB, MeshLab, PolyMender, Ramesh Cleaner, FreeSurfer, and Statistical Parametric Mapping (SPM). We followed the normal model development pathway discussed in the previous section consisting of segmentation, refinement and post-processing with a few modifications, particularly in terms of segmentation. We will now discuss briefly the myriad of individual software tools, both commercial and open source, used in the model development toolchain.

Toolchain

SPM

Statistical Parametric Mapping (SPM, http://www.fil.ion.ucl.ac.uk/spm/), developed by the Wellcome Department of Imaging Neuroscience at University College London, is a software tool used for the analysis of functional MRI data distributed as a MATLAB plugin. Its objective is to investigate the differences in brain activity recorded during fMRIs or PET scans. Voxels are used to describe the map of the area being scanned, independent of which type of imaging software is used. Using statistical data from many prior scanned functional MRI images, the

software package can determine which tissue classes each voxel belongs to and create maps which can be created into surface meshes using other software packages [38].

FreeSurfer

FreeSurfer (https://surfer.nmr.mgh.harvard.edu/), developed at the Athinoula A. Martinos Center for Biomedical Imaging at MGH is a software package whose function is to analyze MRI data to better visualize and map brain images. The most important feature to this project is its ability to produce surface meshes from MRI data [39].

PolyMender

PolyMender (http://www1.cse.wustl.edu/~taoju/code/polymender.htm), a program based on an algorithm developed by Tao Ju in his paper "Robust Repair of Polygonal Models" [40]. PolyMender outputs a closed surface that estimates the input polygonal model. The advantages of PolyMender include a relatively tiny amount of resources required (computer power and time on the researcher's part), while producing a high-quality output consistent with the input geometry.

MeshLab

Meshlab (http://www.meshlab.net/), is an open source software package used to process and improve 3D triangular CAD meshes [41]. It is capable of a multitude of mesh processing functions, but we used it for filetype conversion and Laplacian smoothing in this project.

Ramesh Cleaner

Ramesh Cleaner, developed by Marco Centin and Alberto Signoroni, is a software package designed to improve 3D triangular CAD meshes, mostly tailored for 3D object scanning. Ramesh cleaner is capable of automatically resolving the following common issues with 3D CAD meshes: isolated and degenerate vertices, spikes, fold overs, complex boundaries, self-intersections, holes, micro tunnels, and near-degenerate triangles [37].

Makarov's MATLAB Scripts

Custom MATLAB scripts written by Dr. Sergey Makarov and his lab were heavily utilized in this project. Many of the scripts are described and explained in his book, "Low-Frequency Electromagnetic Modeling for Electrical and Biological Systems Using MATLAB" [42]. Some of the functions performed by these scripts which were utilized in this project include: decimation, Laplacian smoothing, intersection and manifoldness validation, shortest edge decimation, and moving or translating nodes automatically.

ANSYS SpaceClaim

ANSYS SpaceClaim, a 3D CAD modeling software application packaged as part of ANSYS simulation software, is one of the most utilized tools in the toolchain. SpaceClaim is used in any of the manual node and facet manipulations done on the project. As such, hundreds of man-hours were spent in this program correcting meshes and resolving intersections manually. It is also one of the better tools, along with Ramesh Cleaner, for fixing holes, self-intersections, and over-connected edges.

ANSYS Maxwell

ANSYS Maxwell is a Finite Element Analysis software that focuses on electromagnetic field simulation. The software utilizes finite element method techniques to resolve frequency-domain electromagnetic and electric fields [29]. One of the key features of Maxwell is its adaptive meshing which results in faster computation runtime while converging to desired error [29]. The inputs of this software are the object's geometry, material properties, the defined the output of interest, and simulation parameters. The output is a set of data for each point in the model based on the governing equation of interest.

Model Generation Methodology

Semi-Automatic Segmentation

SPM was used to employ its semi-automatic segmentation algorithm in the first round of segmentation for this project. The input to SPM was T1 and T2 MRI images and the output was in the form of a voxel image map for the skin, skull, cerebrospinal fluid (CSF), grey matter (GM), and white matter (WM). We used the default segmentation settings and tissue probability maps with all seven tissue Gaussians specified to capture as much of the geometry as possible. These voxel image maps were imported into FreeSurfer, which allowed us to extract a 3D surface mesh from the voxel image map. This process resulted in a mesh which meets none of the parameters for a 3D CAD surface mesh and has geometry represented inside two (GM, WM) of the mesh shells which was extracted into its own set of 2-manifold meshes.

Decimation and Additional Segmentation

To make meshes easier to work with manually and for performance considerations meshes were decimated after semi-automatic segmentation by an order of 10-100. Custom MATLAB scripts were utilized to perform this operation. SpaceClaim was then utilized to further segment and clean the semi-automatic segmentation from SPM. The output meshes from SPM contained a lot of geometry inside, some of which was captured, and the undesirable portion was deleted. These triangles are deleted because it would violate the rules of a 3D CAD mesh that it must be 2-manifold and non-intersecting while other tissue shells must be fully contained inside the outer tissue layer shell.

The result of this operation was the capture of 3 additional meshes pertaining to the patient's abnormality. These included an edema mesh, and two meshes for the abnormality's inner and outer layer. These layers and edema were identified and correlated to the MRI data viewed in FreeSurfer. An additional round of decimation was performed to approximately reach the target triangle threshold of 125,000 triangles. This number was chosen to estimate a simulation time of about 24-48 hours with 3 adaptive passes through experience with the simulation systems and the ANSYS software platform.

Post-Processing & Mesh Validation

In post-processing, the meshes are smoothed with Laplacian smoothing using either MATLAB or MeshLab to achieve the same result. At this point, we had isolated the geometry, decimated it to the required number of triangles, and improved triangle quality using Laplacian smoothing. The next step in the process was mesh validation. The individual meshes were validated in SpaceClaim and corrected of the countless triangle problems that can occur, such as

holes, as was discussed in the CEM model background section. Triangle quality is also an important consideration at this stage and MATLAB scripts were utilized to improve the overall triangle quality of some meshes.

The skull mesh was especially difficult to achieve adequate triangle quality and produce an accurate mesh. This is due to the complex geometry of the skull's orbital bones and sinus cavities. As a result, the team spent the greatest amount of time on the skull model. PolyMender was employed to generate a new mesh for the GM which improved the mesh processing and validation time from tens of hours to just one or two. The PolyMender algorithm was not effective when applied to the skull model, especially when compared to the success of the GM, again likely due to its complex geometry.

After the individual meshes are validated, they must all be placed into ANSYS Maxwell for a more rigorous individual mesh validation and validation of the model as whole by checking for intersections between meshes in and around contact regions. This took the second greatest amount of time to complete. When intersections are indicated in ANSYS Maxwell's validation procedure, they must then be located by inspection in SpaceClaim. Once the triangles of interest are located, nodes are moved or, facets are deleted and recreated, to resolve the intersection. This process repeats for each intersection in each mesh until all are resolved and validation is successful inside ANSYS Maxwell. If large area of intersection was detected, MATLAB scripts were used to attempt to automatically resolve the intersections. It achieved this result by moving nodes slightly and checking for intersections in an automated fashion with somewhat limited results. The fastest way to resolve intersections is manually. A flow chart of the process explained above is available in Fig. 7.

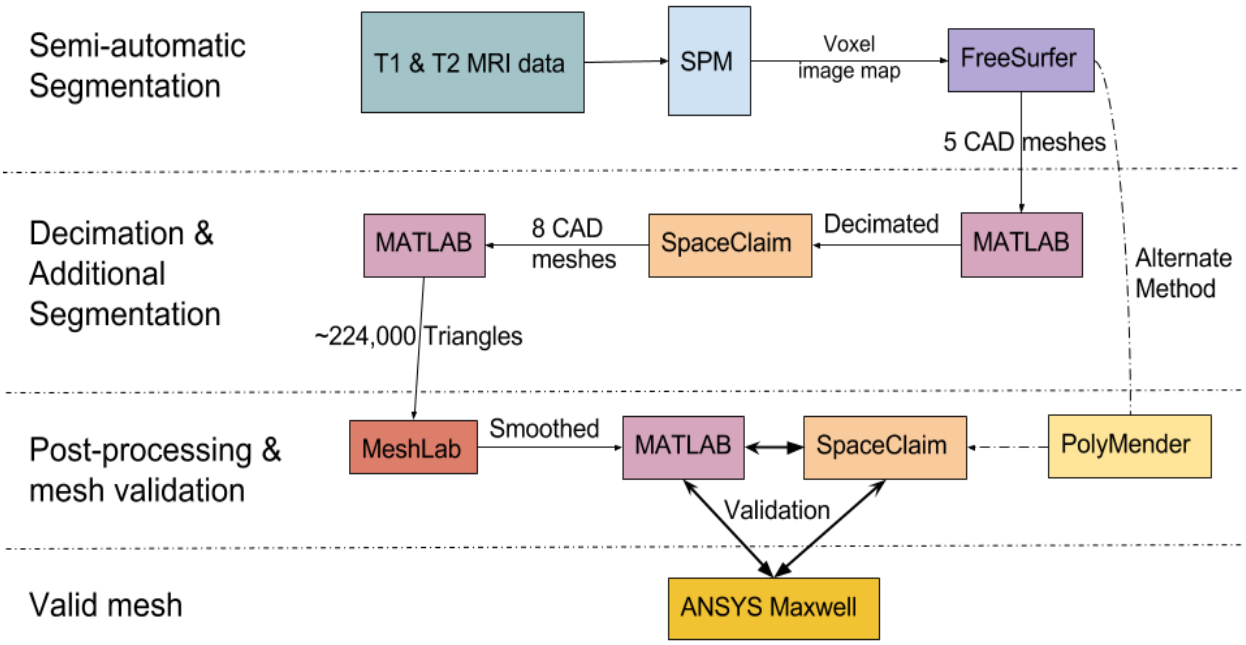

Figure 7. Flow chart of model development procedure with toolchain items in boxes and arrows labeled with processes.

Model Results

The resulting final meshes have the following properties:

- All meshes are strictly 2-manifold
- All meshes do not intersect
- Referring to Table 2, meshes 2 through 8 are contained within the skin mesh
- Meshes 4 through 8 are contained within the CSF mesh
- Meshes 5 through 8 are contained within the GM mesh
- Meshes 7 and 8 are contained within the Edema mesh
- Mesh 8 is within the Tumor (outer) mesh

Table 2 contains the relevant statistics for each mesh. The final total number of triangles in the model is 134,171. Each individual mesh is presented in Fig. 8-15. A cross-section of the entire model with each tissue mesh labeled is available in Fig. 16.

Mesh	Num. of triangles	Min. triangle quality	Min. edge length (mm)
01 SKIN	9982	0.06	0.64
02 SKULL	27668	0.0002	0.10
03 CSF	5992	0.03	0.72
04 GM	25000	0.03	0.45
05 WM	49044	0.02	0.37
06 EDEMA	7530	0.06	0.18
07 TUMOR OUTER	3732	0.02	0.16
08 TUMOR INNER	5332	0.11	0.12

Table 2. Model results tabulation including mesh name, number of triangles, minimum triangle quality, and minimum edge length.

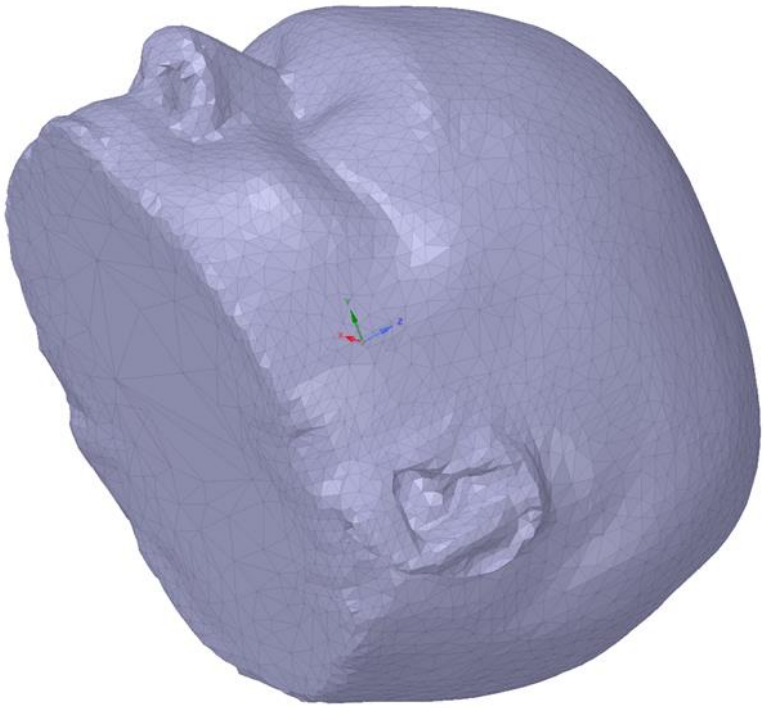

Figure 8. Completed and validated 3D CAD surface mesh of the skin, which contains 9,982 triangles.

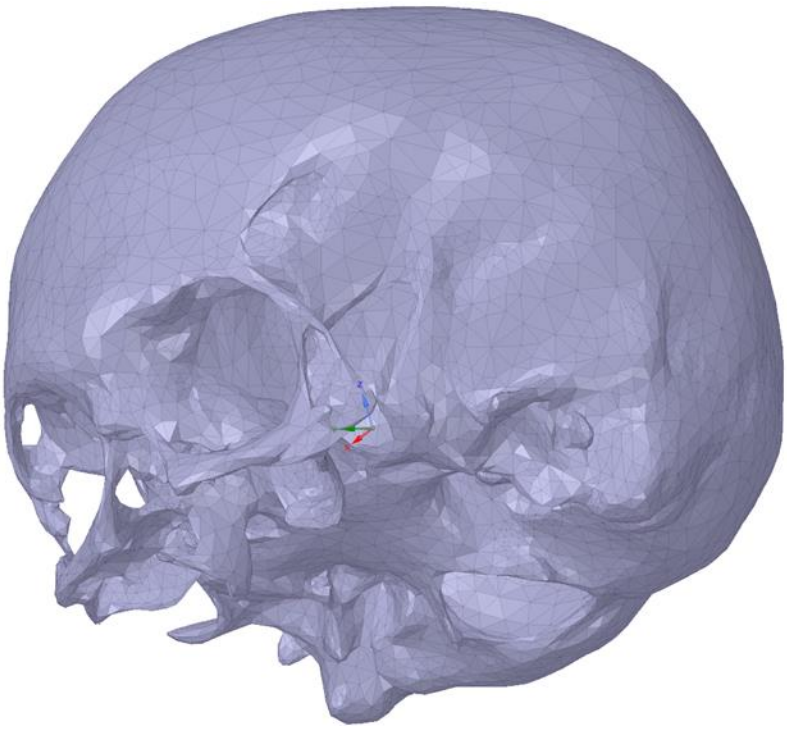

Figure 9. Completed and validated 3D CAD surface mesh of the skull, which contains 27,668 triangles.

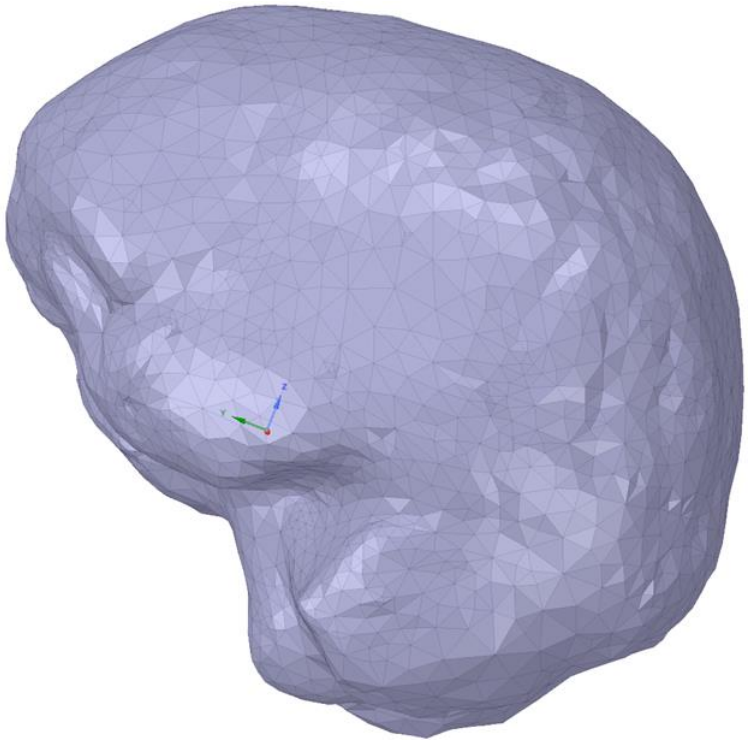

Figure 10. Completed and validated 3D CAD surface mesh of the CSF, which contains 5,992 triangles.

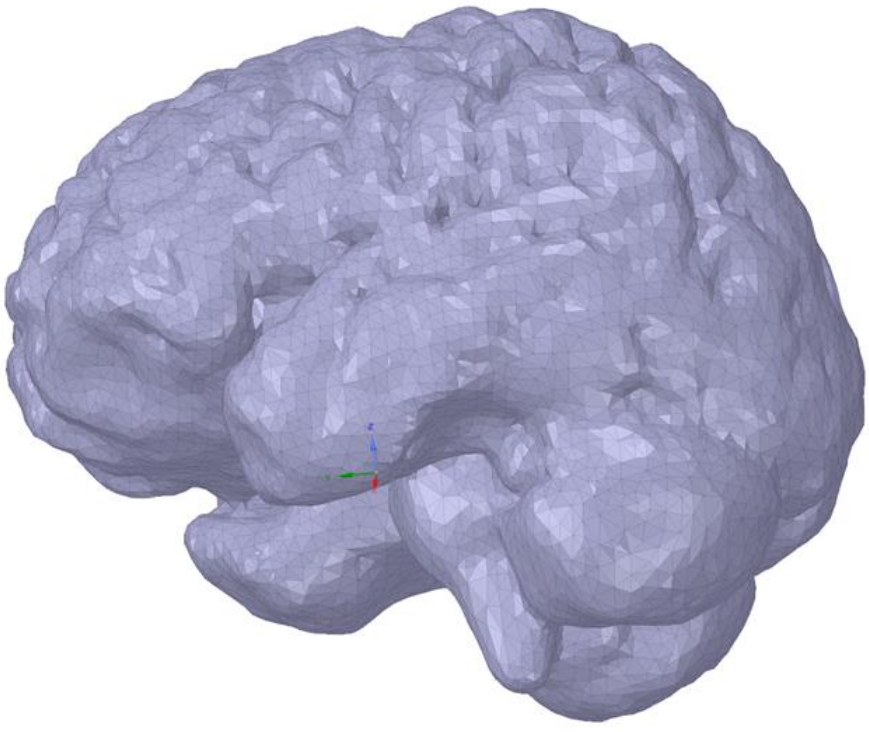

Figure 11. Completed and validated 3D CAD surface mesh of the GM, which contains 25,000 triangles.

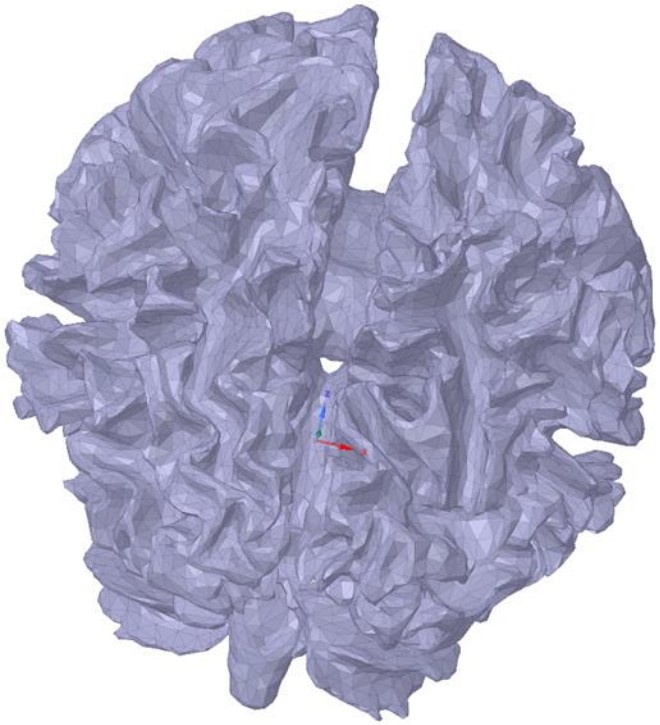

Figure 12. Completed and validated 3D CAD surface mesh of the WM, which contains 49,044 triangles.

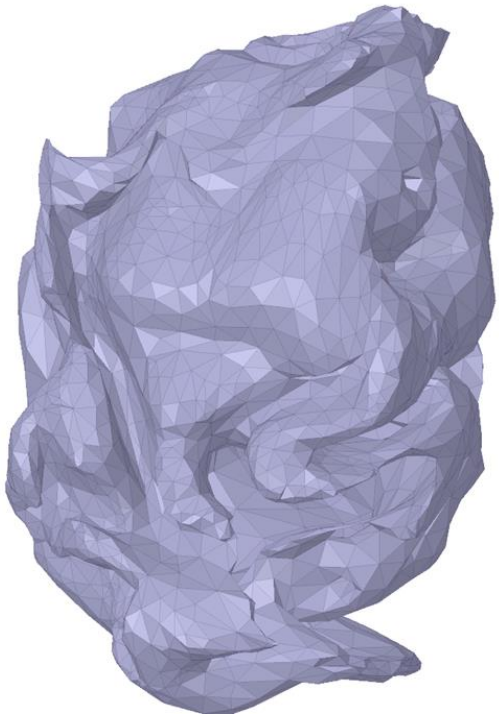

Figure 13. Completed and validated 3D CAD surface mesh of the edema, which contains 7,530 triangles.

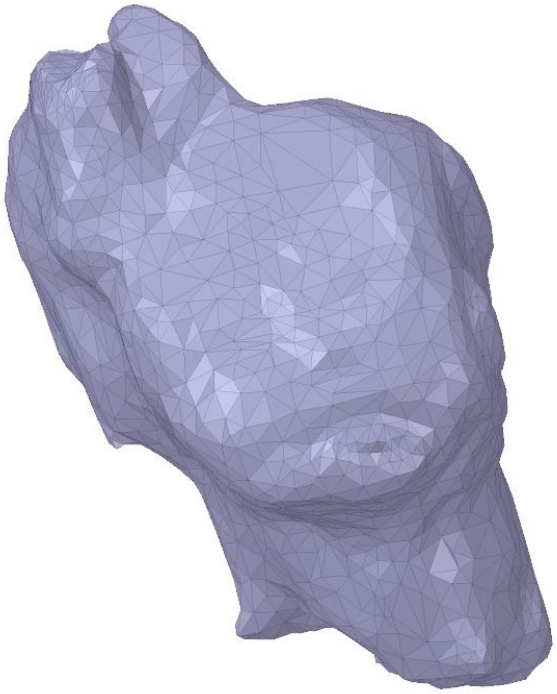

Figure 14. Completed and validated 3D CAD surface mesh of the tumor (outer), which contains 3,732 triangles.

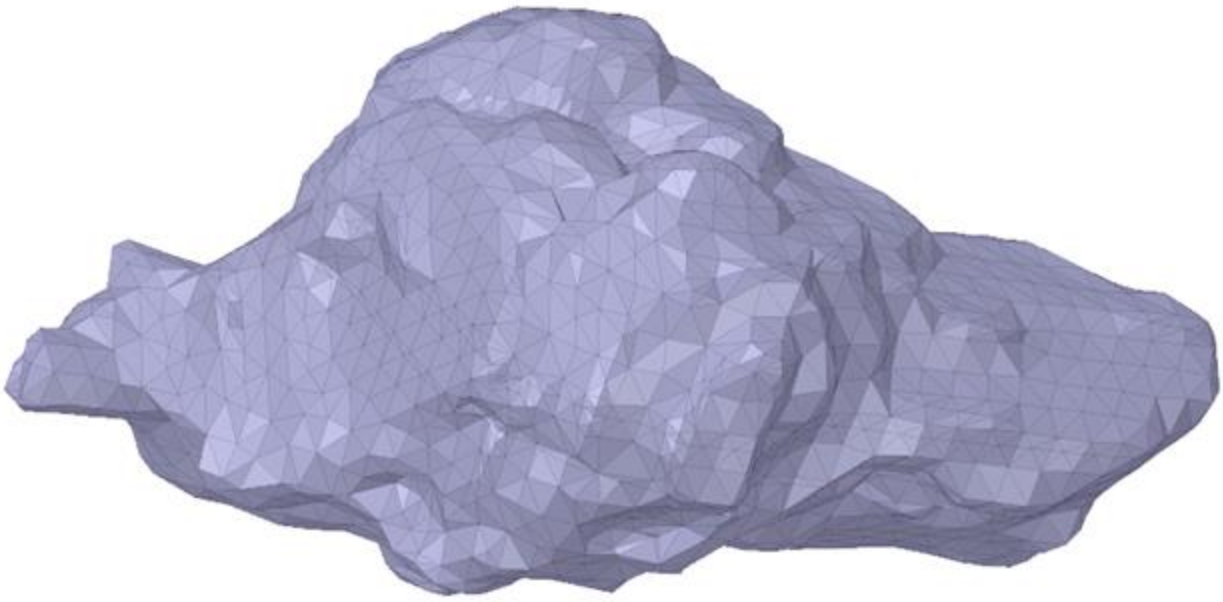

Figure 15. Completed and validated 3D CAD surface mesh of the tumor (inner), which contains 5,332 triangles.

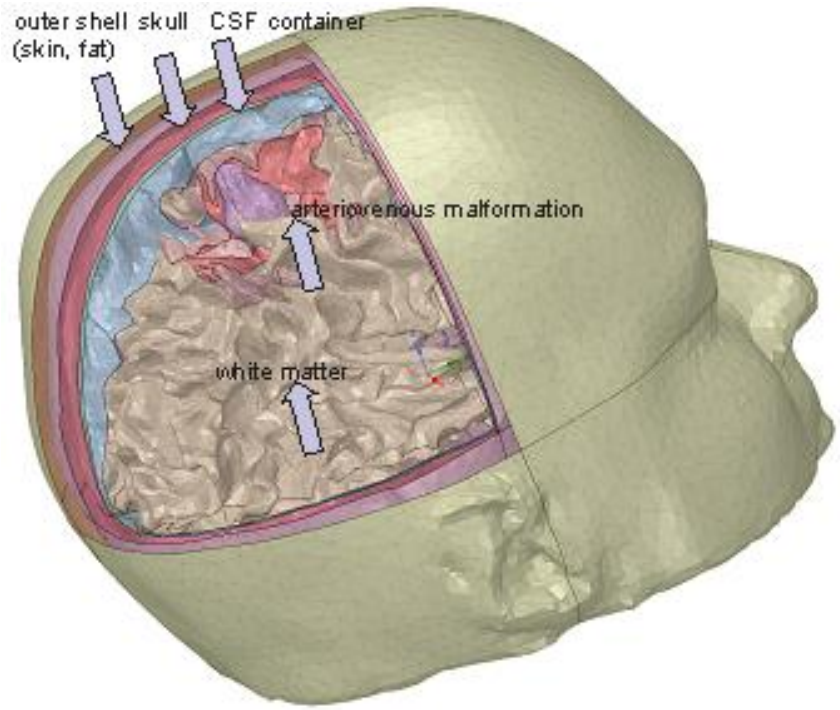

Figure 16. Full head model cross-section with visible tissue mesh layers labeled.

Rapid Modeling Recommendation

My recommendation for rapid mesh generation is to create a custom solution for surface mesh extraction from the SPM voxel image maps. A lot of time and effort could be saved by producing a higher-quality mesh at the conversion step. If that is not possible, I would recommend the use of PolyMender directly after FreeSurfer mesh generation. It generates an entirely new surface mesh where you can designate the desired resolution and it aims to create a manifold, water-tight shell. From Tao Ju's paper, Robust Repair of Polygonal Models, "The method is guaranteed to produce a closed surface that partitions the space into disjoint internal and external volumes" [40]. Using this as a starting point for post-processing saves an incredible amount of time especially on meshes like the skin, CSF, GM and WM. The skull was less

successful with this method due to its complexity (i.e. sinus cavities and orbital bones). Ramesh Cleaner along with manual correction in SpaceClaim were the two tools most useful for the creation and refinement of the skull mesh.

Simulation in ANSYS Maxwell

For the simulation of this project ANSYS Maxwell was used. An Eddy current simulation was performed with a 5 kHz sine wave from a 1 kA excitation at the modeled coil directed to the cortex. The setup for the simulation consisted of creating the coil geometry (radius 2.5cm), setting the dielectric properties for the materials (including air), importing and validating all the meshes in ANSYS Maxwell, including resolving inter-mesh intersections and inverted triangles. We set the simulation to run on 8 cores for 3 adaptive passes for a final mesh of approximately 1,000,000 tetrahedra. With these parameters, the simulation took about a day to run. We then create the images by cutting through the model at various depths to display the E field on that plane for presenting to MGH researchers.

Simulation Parameters

We carried out two simulations to demonstrate the effect the patient's abnormality had on the **E** field in his cortex. In the first simulation, the edema, tumor (outer), and tumor (inner) were set to the same values as WM, with permittivity of 2.09E+4 and a conductivity of 1.10E-1, as shown in Table 1. This provides a simulation on the patient's geometry with the WM as one

homogeneous region. Essentially, his abnormality can be considered not present in the "normal" simulation results. Other tissues were set to their appropriate values as per Table 1.

The second simulation contains the abnormal properties for edema, tumor (outer), and tumor (inner). Edema is assigned an average of blood and WM (1.77e4, 3.83e-1); Tumor (inner), and Tumor (outer) are both assigned blood properties as per Table 1. These choices for conductivity and permittivity tissue value assignments were made in consultation with medical researchers and professionals at MGH. An Eddy current simulation was performed for each of the two models with a 5 kHz sine wave from a 1 kA excitation at the modeled coil. Each simulation was set to run for 3 adaptive passes.

Coil Model Generation

More accurate coil development was attempted and is shown in Fig. 17. It was created in ANSYS Maxwell and replicated the Magstim coil used in the actual procedure. Copper tape was created with a small insulating layer of plastic around it and wound for 8 turns. It was not used in favor of the simple figure-8 coil because the figure-8 is the accepted standard for TMS FEA simulations.

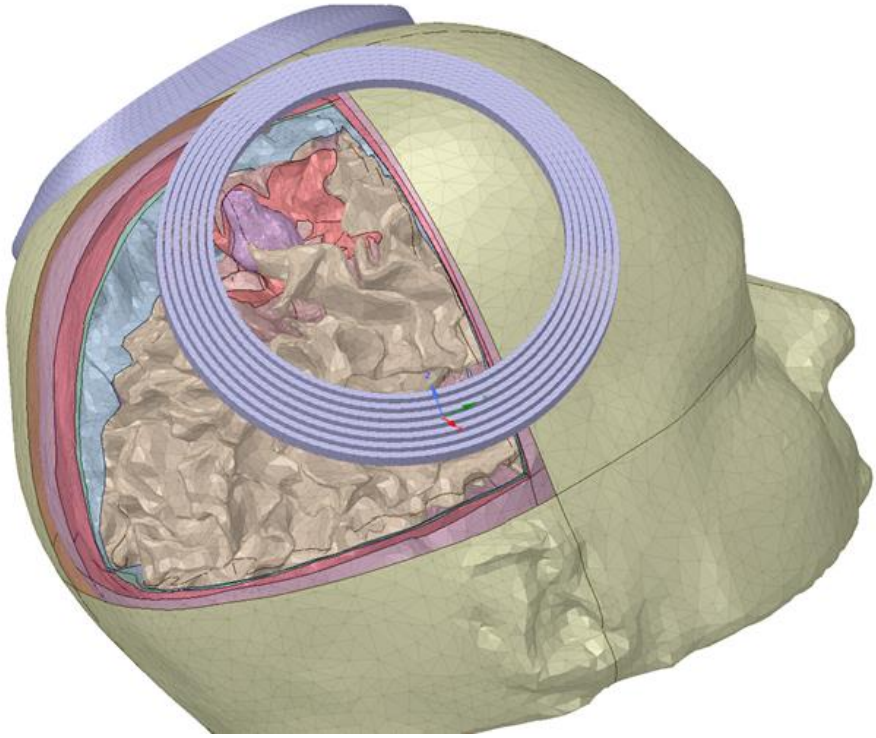

Figure 17. Full head model cross section with accurate copper-tape coil representation.

Simulation Results

The simulations ran for approximately 24 hours on 8 cores of a HPC Linux sever. The models were cross-sectioned in 15mm intervals through the region of the patient's abnormality. Fig. 18 illustrates the cross-sectioning and shows the location of the abnormality as it was cross-sectioned. Edema is colored magenta, tumor (outer) is colored green, and tumor (inner) is colored red. On each of these cross-sections from both simulations, the **E** field is plotted as a heat map across the plane of the cerebrum. On each of the following comparison figures, a box has been drawn around the location of the patient's abnormality. Figures 19 and 20 show the comparison of "normal" and "abnormal" at a depth of 65mm from the top of the scalp. There is a clear increase in the **E** field in the location of the abnormality in the "abnormal"

simulation. In Figures 21 and 22, we move up to a depth of 50mm in the patient's cortex. The increase in the **E** field in the region of the abnormality follows what we saw at the previous depth. Now, notice there is also a large gradient between the various layers of the abnormality. Moving to a depth of 35mm in Figures 23 and 24 we continue to see the same trend.

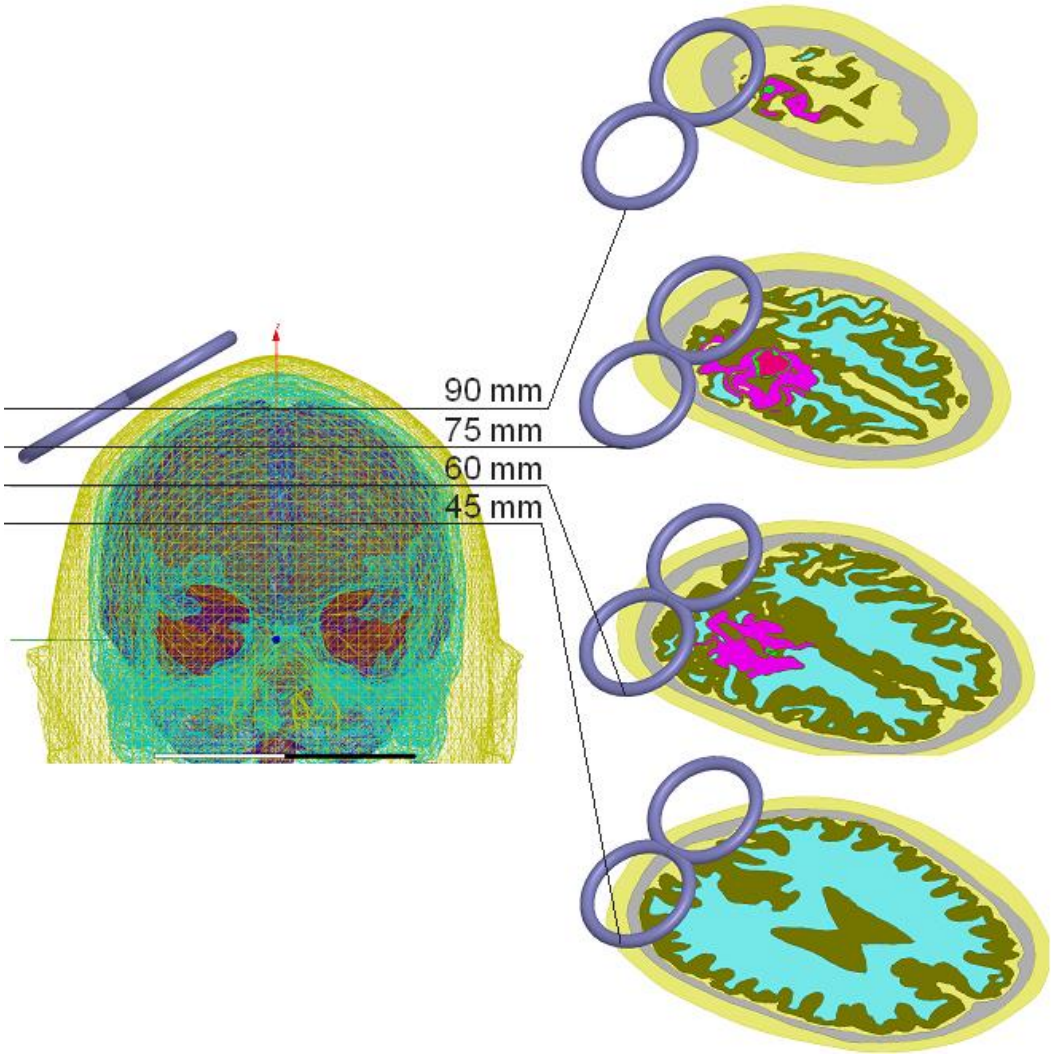

Figure 18. Full head model cross-sections showing relative height of the visualizations from the origin (the origin is in the center of the skull).

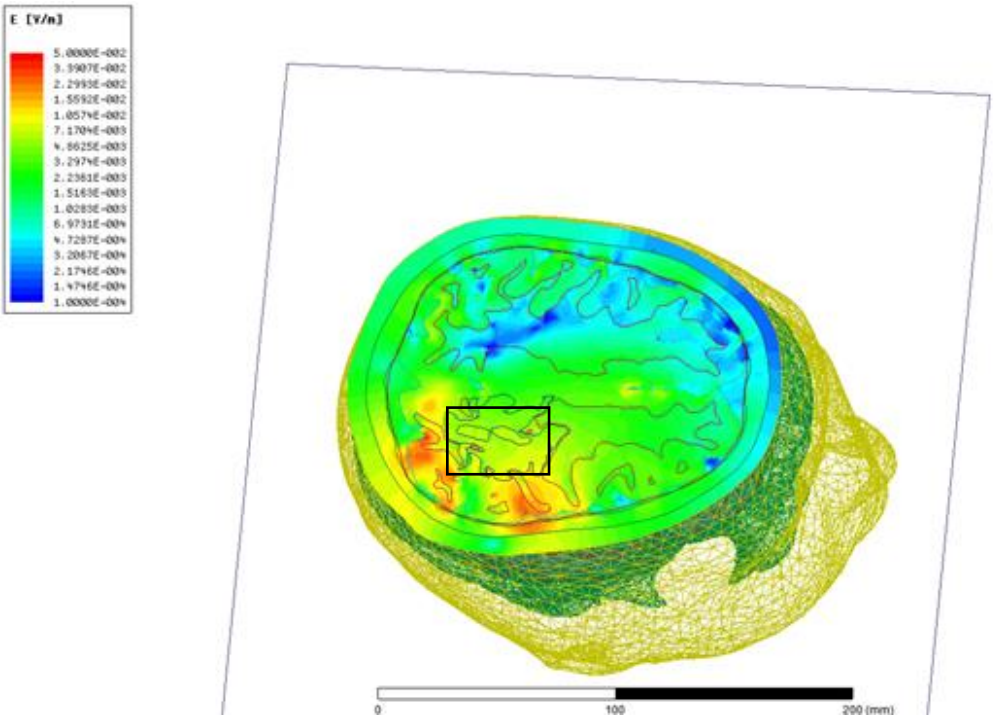

Figure 19. Cross-section of the "normal" head model at 65mm depth from the scalp with the ***E*** *field plotted in V/mm.*

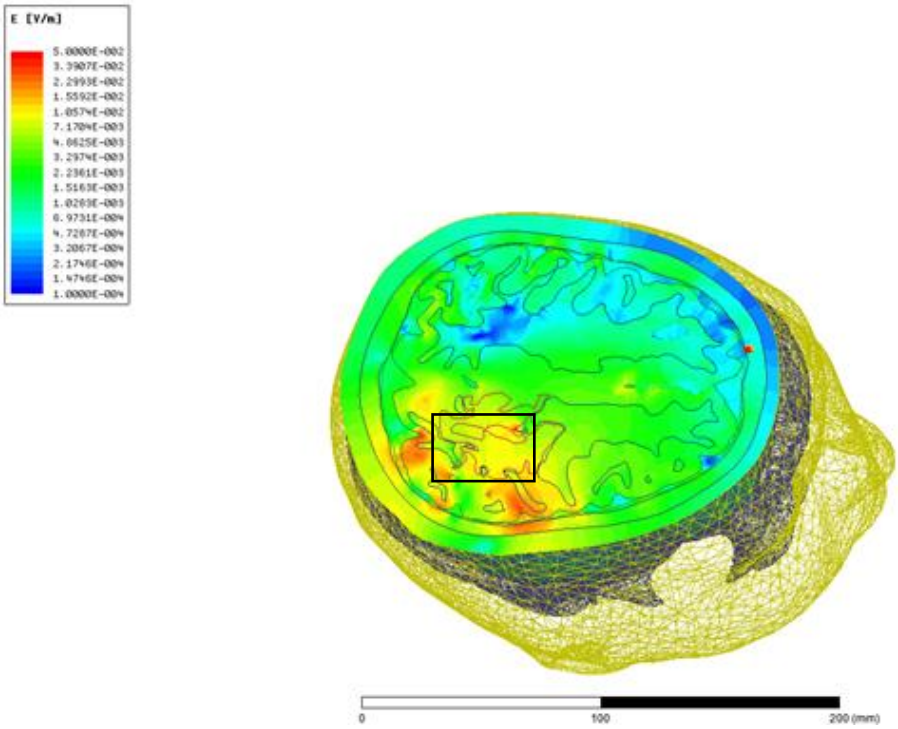

Figure 20. Cross-section of the "abnormal" head model at 65mm depth from the scalp with the ***E*** *field plotted in V/mm.*

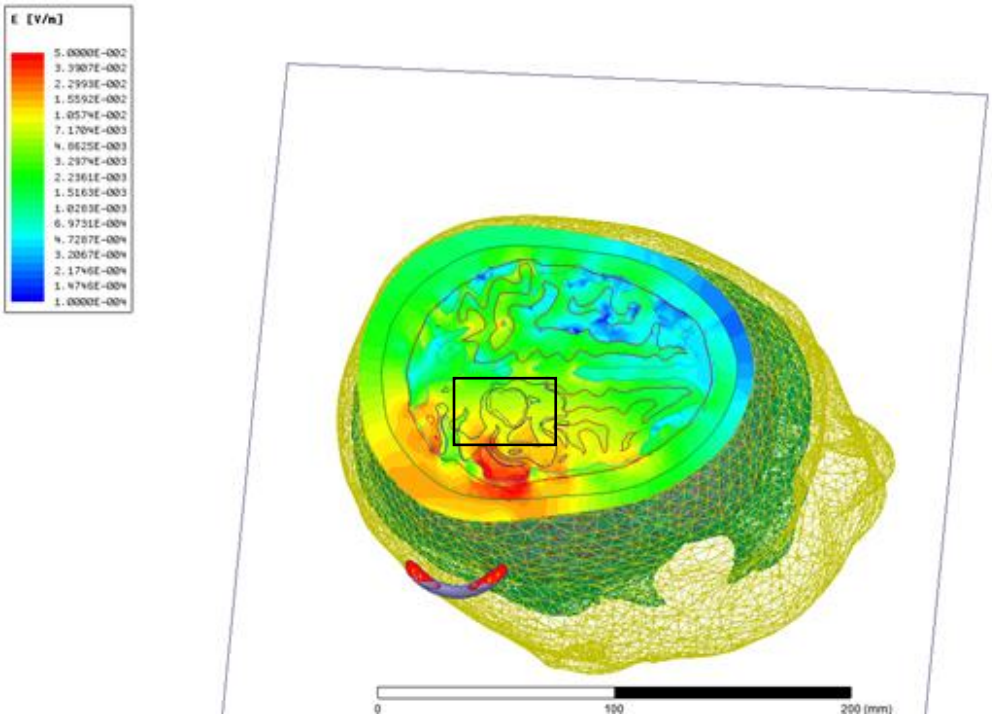

*Figure 21. Cross-section of the "normal" head model at 50mm depth from the scalp with the **E** field plotted in V/mm.*

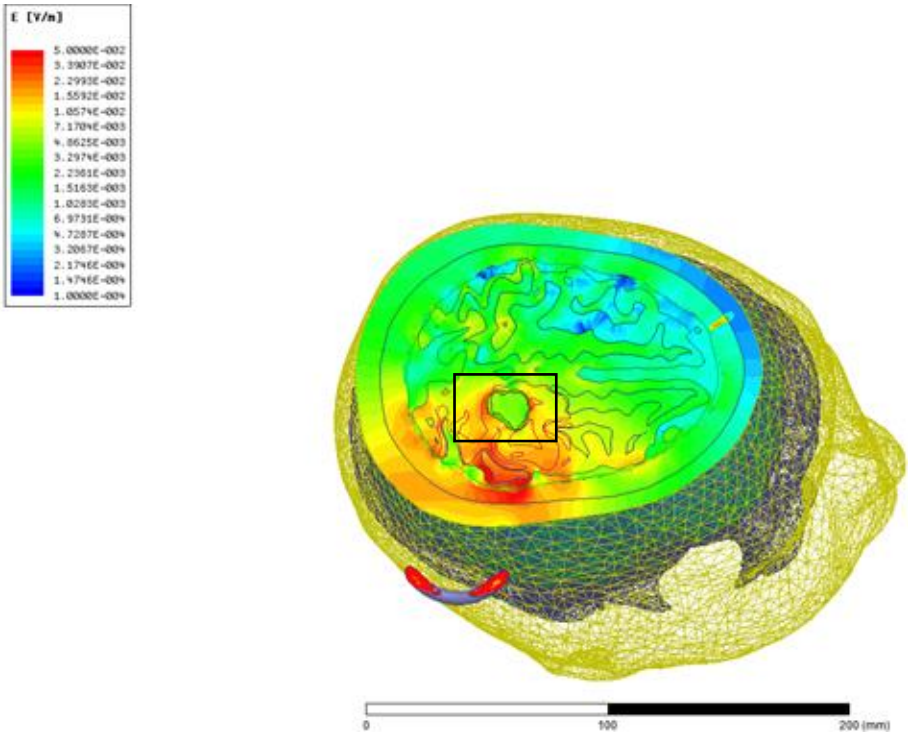

*Figure 22. Cross-section of the "abnormal" head model at 50mm depth from the scalp with the **E** field plotted in V/mm.*

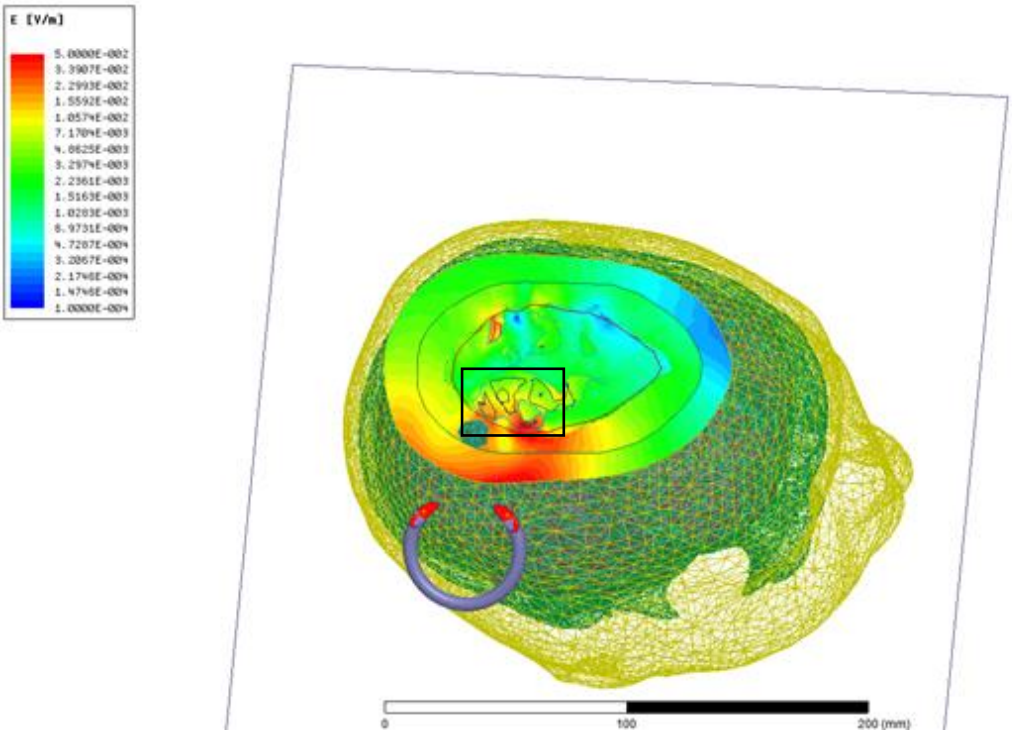

*Figure 23. Cross-section of the "normal" head model at 35mm depth from the scalp with the **E** field plotted in V/mm.*

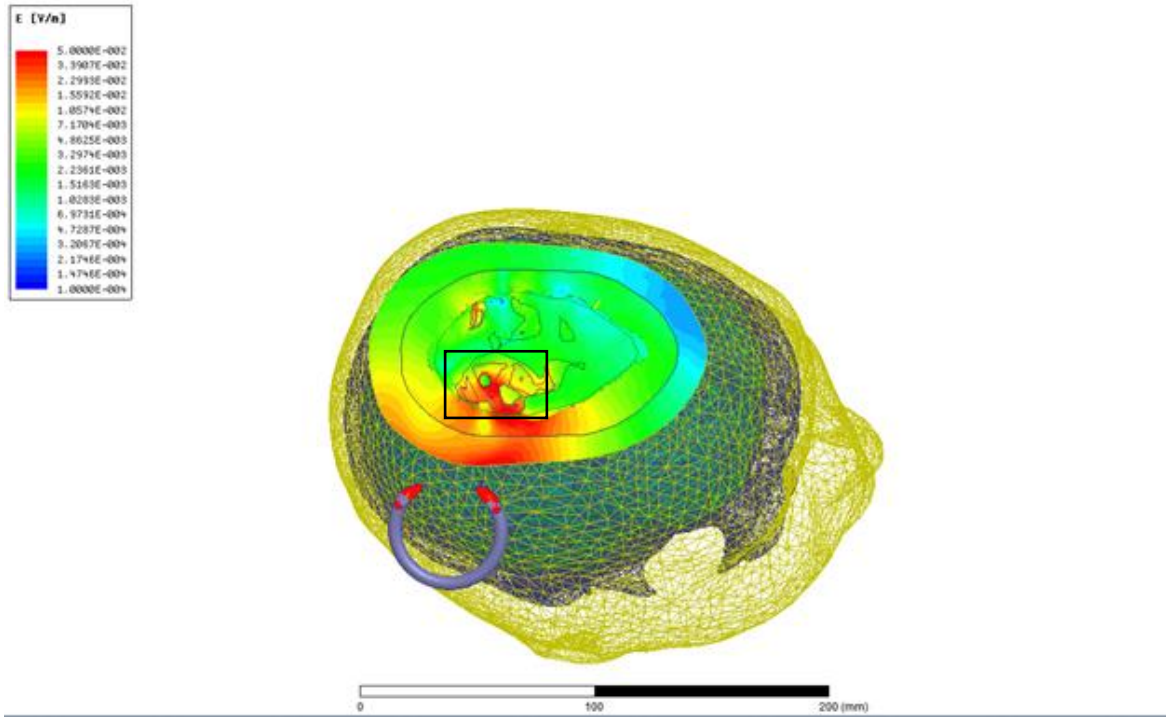

*Figure 24. Cross-section of the "abnormal" head model at 35mm depth from the scalp with the **E** field plotted in V/mm.*

Conclusions and Future Work

The purpose of this Major Qualifying Project was to create an accurate model of the patient's head from T1 and T2 MRI images, which was completed successfully. ANSYS Maxwell was used to conduct a finite element analysis of patient's unique cranial geometry to calculate the electric field inside the cortex during a simulated TMS procedure. The results were plotted showing the abnormality indeed does have an impact on the **E** field in the patient's brain during a simulated TMS procedure. Additionally, this project made recommendations for the process of rapid 3D surface mesh generation from T1 and T2 MRI images. Future work may include formalizing these recommendations into a procedure that includes PolyMender or a custom converter from the output of SPM designed with meeting the requirements of FEA 3D surface meshes as the goal.

References

[1] P. M. Rossini et al., “Non-invasive electrical and magnetic stimulation of the brain, spinal cord, roots and peripheral nerves: Basic principles and procedures for routine clinical and research application. An updated report from an I.F.C.N. committee,” Clin. Neurophysiol., vol. 126, no. 6, pp. 1071–1107, Jun. 2015.

[2] A. T. Barker, I. L. Freeston, R. Jalinous, P. A. Merton, and H. B. Morton, “Magnetic stimulation of the human brain,” J. Physiol. (Lond.), vol.369, p. 3P, 1985.

[3] S. Rossi et al., “Safety of TMS consensus group, ethical considerations, and application guidelines for the use of transcranial magnetic stimulation in clinical practice and research,” Clin. Neurophysiol., vol. 120, no. 12, pp. 2008–2039, Dec. 2009.

[4] Jalinous R., “Technical and practical aspects of magnetic nerve stimulation,” J. Clin. Neurophysiol 1991; 8:10–25.

[5] Thielscher A, Kammer T. “Electric field properties of two commercial figure-8 coils in TMS: calculation of focality and efficiency,” Clin. Neurophysiol 2004; 115: 1697–708

[6] Rossi S, Hallett M, Rossini PM, Pascual-Leone A. “Safety, ethical considerations, and application guidelines for the use of transcranial magnetic stimulation in clinical practice and research,” Clin. Neurophysiol 2009; 120: 2008–39.

[7] Mould, S. U.S. Patent 6,179,770, 2001.

[8] L. J. Gomez. “Computational electromagnetic methods for transcranial magnetic stimulation,” 2015.

[9] Lefaucheur, JP; et al. "Evidence-based guidelines on the therapeutic use of repetitive transcranial magnetic stimulation (rTMS)," Clinical Neurophysiology. 2014; 125 (11): 2150–2206.

[10] D. R. Kimetal.,“A survey of patient acceptability of repetitive transcranial Magnetic stimulation (TMS) during pregnancy,” J. Affect Disord., vol. 129, nos. 1–3, pp. 385–390, Mar. 2011.

[11] Groppa, S. et al. “A practical guide to diagnostic transcranial magnetic stimulation: Report of an IFCN committee,” Clinical Neurophysiology, Vol. 123 , Issue 5 , 858 – 882.

[12] Ruohonen J, Ilmoniemi R J. “Physical principles for transcranial magnetic stimulation,” In: Pascual-Leone A, Davey NJ, Rothwell J, Wassermann EM, Puri BK, editors. Handbook of transcranial magnetic stimulation. New York: Oxford University Press; 2002.

[13] Brix G, Seebass M, Hellwig G, Griebel J. Estimation of heat transfer and temperature rise in partial-body regions during MR procedures: an analytical approach with respect to safety considerations. Magn Reson Imag 2002; 20:65–76.

[14] Roth BJ, Pascual Leone A, Cohen LG, Hallett M. "The heating of metal-electrodes during rapid-rate magnetic stimulation – a possible safety hazard," Electroenceph Clin Neurophysiol 1992;85:116–23.

[15] Gandhi OP. Electromagnetic fields: human safety issues. Annu Rev Biomed Eng 2002; 4:211–34

[16] Bae EH, Schrader LM, Machii K, Alonso-Alonso M, Riviello Jr JJ, Pascual-Leone A, et al. "Safety and tolerability of repetitive transcranial magnetic stimulation in patients with epilepsy: a review of the literature," Epilepsy Behavior 2007;10:521–8.

[17] Rossi, Simone Hallett, Mark Rossini, Paolo M., Pascual-Leone, Alvaro et al. "Screening questionnaire before TMS: An update," Clinical Neurophysiology, Volume 122, Issue 8

[18] Fitzgerald PB, Hoy K, McQueen S, Maller JJ, Herring S, Segrave R, et al. "A randomized trial of rTMS targeted with MRI based neuro-navigation in treatment-resistant depression," Neuropsychopharmacology 2009;34:1255–62.

[19] ICNIRP, "Guidelines for limiting exposure to time-varying electric, magnetic and electromagnetic fields (up to 300 GHz)," Health Phys., vol. 74, no. 4, pp. 494–522, Apr. 1998.

[20] ICNIRP, "Guidelines for limiting exposure to time-varying electric and magnetic fields (1 Hz–100 kHz)," Health Phys., vol. 99, no. 6, pp. 818–836, Dec. 2010.

[21] National Institute of Biomedical Imaging and Bioengineering, NIH: "Computational Modeling," July 2013.

[22] U.S. Food and Drug Administration, Center for Devices and Radiological Health "Reporting of Computational Modeling Studies in Medical Device Submissions: Draft Guidance for Industry and Food and Drug Administration Staff," Jan 17th, 2014.

[23] ZJ Cendes, "Vector Finite Elements for Electromagnetic Field Computation," IEEE Transactions on Magnetics, vol. MAG-27, pp. 3953-3966, 1991.

[24] Jin, J., "The finite element method in electromagnetics." Vol. 2nd. 2002, New York: Wiley.

[25] Volakis, J.L., A. Chatterjee, and L.C. Kempel, "Finite element method for electromagnetics: antennas, microwave circuits, and scattering applications." 1998, New York: IEEE Press

[26] J. Hesthaven and T. Warburton, “Nodal Discontinuous Galerkin Methods Algorithms, Analysis, and Applications, Springer series: Texts In Applied Mathematics”, vol.54, 2007.

[27] U.S. Food and Drug Administration, Center for Devices and Radiological Health “Reporting of Computational Modeling Studies in Medical Device Submissions: Draft Guidance for Industry and Food and Drug Administration Staff,” Jan 17th, 2014.

[28] Computational human phantom, Wikipedia. Available: https://en.wikipedia.org/wiki/Computational_human_phantom

[29] Makarov SN, Noetscher GM, Yanamadala J, et al. “Virtual Humans Models for Electromagnetic Studies and Their Applications,” 2016

[30] W. P. Segars, G. Sturgeon, S. Mendonca, J. Grimes, and B. M. W. Tsui,, “4D XCAT phantom for multimodality imaging research,” Med. Phys.,vol. 37, no. 9, pp. 4902-4915, 2010.

[31] K. Genc et al., “Workflow for creating a simulation ready virtual population for finite element modeling,” J. Med. Devices, vol. 7, no. 4, Dec. 2013.

[32] 29M. Sezgin and B. Sankur, “Survey over image thresholding techniques and quantitative performance evaluation,” Journal of Electronic Imaging, vol. 13, no. 11, pp. 46-165, Jan. 2004.

[33] M. Garland and P. S. Heckbert, “Surface simplification using quadric error metrics,” 24th Annual Conf. on Computer Graphics and Interactive Techniques. pp. 209-216. 1997.

[34] C. Gabriel. “Compilation of the Dielectric Properties of Body Tissues at RF and Microwave Frequencies,” Report N.AL/OE-TR- 1996-0037, Occupational and environmental health directorate, Radiofrequency Radiation Division, Brooks Air Force Base, Texas (USA), 1996.

[35] R. V.Garimella et al., “Triangular and Quadrilateral Surface Mesh Quality Optimization Using Local Parametrization,” Comput. Methods in Applied Mechanics and Eng., vol. 193, no. 9–11, pp. 913–928, Mar. 2004

[36] D. Field, “Laplacian smoothing and Delaunay triangulations,” Communications in Applied Numerical Methods, vol. 4, pp. 709–712 1998.

[37] M Centin, A Signoroni; “Ramesh Cleaner: Conservative Fixing of Triangular Meshes”, 2015

[38] Friston, K.J., “Statistical parametric mapping,” 1994

[39] Fischl, B., “FreeSurfer,” Neuroimage, 62(2), pp.774-781. 2012

[40] Ju, T., “Robust repair of polygonal models,” ACM Transactions on Graphics (TOG), 23(3), pp.888-895. 2004

[41] Cignoni, P., Corsini, M. and Ranzuglia, G., “Meshlab: an open-source 3d mesh processing system,” Ercim news, 73(45-46), p.6. 2008

[42] Makarov, S.N., Noetscher, G.M. and Nazarian, A., “Low-Frequency Electromagnetic Modeling for Electrical and Biological Systems Using MATLAB,” John Wiley & Sons. 2015

[43] Awiszus, F., “TMS and threshold hunting.” Supplements to Clinical neurophysiology, 56, pp.13-23. 2003.

[44] Rusjan, P.M., Barr, M.S., Farzan, F., Arenovich, T., Maller, J.J., Fitzgerald, P.B. and Daskalakis, Z.J., “Optimal transcranial magnetic stimulation coil placement for targeting the dorsolateral prefrontal cortex using novel magnetic resonance image-guided neuronavigation.” Human brain mapping, 31(11), pp.1643-1652. 2010.